Check for updates

ASCE

Near-Full-Scale Hydraulic Modeling of Fish-Friendly Culvert with Full-Height Sidewall Baffles

Jiayue Hu[1]; Youkai Li[2]; and Hubert Chanson[3]

Abstract: The adoption of baffles is relatively common in the construction of culverts, to assist with the upstream passage of migrating fish species. However, there still is a lack of systematic studies of the complicated hydraulic conditions induced by the baffles to optimize the designs. Herein, near-full-scale physical modeling was performed, focusing on the oscillation and instability of open-channel flow in a fish-friendly culvert equipped with full-height sidewall baffles. High-resolution measurements of the instantaneous flow velocity were obtained using an acoustic Doppler velocimeter. The physical results were marked by the existence of some low-frequency oscillations. A triple decomposition technique was applied to the free-surface and velocity time series. The low-pass components confirmed a unique flow structure, consisting of a high-velocity zone in the main channel and a low-velocity flow reversal within the lateral cavities. The band-pass components corresponded to the low-frequency flow oscillations, highlighting the complicated transverse interactions between the lateral cavity and the main channel. The high-pass velocity components were related to the true turbulence characteristics. This study provides a quantitative data set in support of the sustainable design of culverts to assist with upstream fish migration in artificial and natural fast waterways. **DOI: 10.1061/JHEND8.HYENG-13752.** © *2024 American Society of Civil Engineers.*

Author keywords: Physical modeling; Sidewall baffle; Fish-friendly culvert; Hydrodynamics; Triple decomposition.

Introduction

Fish migration commonly occurs in natural waterways as a natural phenomenon. In eastern Australia, road crossings constitute a major hinderance for the upstream passage of small-bodied fish species and juveniles of large fish, which usually are less than 100 mm in total length and have very limited swimming performances, typically with characteristic swimming speeds less than 0.3 m/s (Chanson and Leng 2021). In the State of Queensland alone, there are more than 12,000 such barrier structures that may prevent fish migrations (Dutton et al. 2021). Their negative effect on native fish species and biodiversity cannot be neglected, and some agreement tends to suggest that the high water velocities affect the upstream passage of small-body weak-swimming fish most adversely (Pavlov et al. 1994; Chanson and Leng 2021).

For both stream rehabilitations and new artificial developments, baffles may be installed on the invert and walls to achieve flow conditions that can assist fish with upstream migration (Rajaratnam et al. 1991; Enders et al. 2017; Duguay et al. 2019). Full-height sidewall baffles (Fig. 1) have been observed to facilitate the upstream passage of a number of small-bodied Australian fish species and juveniles of larger fish in standard box culverts (Marsden 2015). At low flow rates, the baffles reduce the water velocity, increase the flow depth, and provide rest areas, all of which facilitate upstream fish migration (Cahoon et al. 2007; Duguay and Lacey 2014). Although some consensus suggests that the high flow velocity in artificial waterways commonly is a physical challenge for small weak-swimming fish travelling upstream, the performance of baffles facilitating fish movement is related closely to the targeted fish guilds and species (Pavlov et al. 1994; Enders et al. 2017; Jones et al. 2020). In addition, the introduction of sidewall baffles may create excessive turbulence at some flow conditions, which can hinder fish movement and passage (Nikora et al. 2003; Cote and Webb 2015).

The presence of the lateral cavities between consecutive baffles may create strong coherent structures in the separated shear zones, as reported by Valentine and Wood (1979) and Hill (2014). The hydrodynamic instabilities may be highly coherent when some coupling occurs between the separation layer and the natural wave modes in the channel and lateral cavity (Tuna et al. 2013). In particular, sidewall baffles were observed to adversely impair the discharge capacity of culvert structures, and might cause turbulent hydrodynamic instabilities in the barrel (Leng and Chanson 2020a, b). Moreover, although some field trials of sidewall-baffled culverts were conducted, the extents of the tests and investigated flow conditions were limited to very low flows (Marsden 2015; Dutton et al. 2021). Thus, there is a need for a more robust hydraulic engineering analysis covering a wide range of flow levels in culverts equipped with full-height sidewall baffles.

In this study, new laboratory experiments were performed at the University of Queensland, in a relatively large and near-full-scale fish-friendly culvert model (Hu et al. 2022). The focus of the measurements was the instabilities of the water surface and water velocities, as well as the coupling between free-surface and velocity fluctuations in the presence of full-height sidewall baffles. The outcomes are expected to provide a quantitative data set to support

[1]Research Student, School of Civil Engineering, Univ. of Queensland, Brisbane, QLD 4072, Australia. ORCID: https://orcid.org/0000-0003-4295-7217

[2]Research Fellow, School of Civil Engineering, Univ. of Queensland, Brisbane, QLD 4072, Australia (corresponding author). ORCID: https://orcid.org/0000-0002-4281-5457. Email: youkai.li@uq.edu.au

[3]Professor in Hydraulic Engineering, School of Civil Engineering, Univ. of Queensland, Brisbane, QLD 4072, Australia, ORCID: https://orcid.org/0000-0002-2016-9650. Email: h.chanson@uq.edu.au

Note. This manuscript was submitted on May 4, 2023; approved on January 3, 2024; published online on March 25, 2024. Discussion period open until August 25, 2024; separate discussions must be submitted for individual papers. This paper is part of the ***Journal of Hydraulic Engineering***, © ASCE, ISSN 0733-9429.

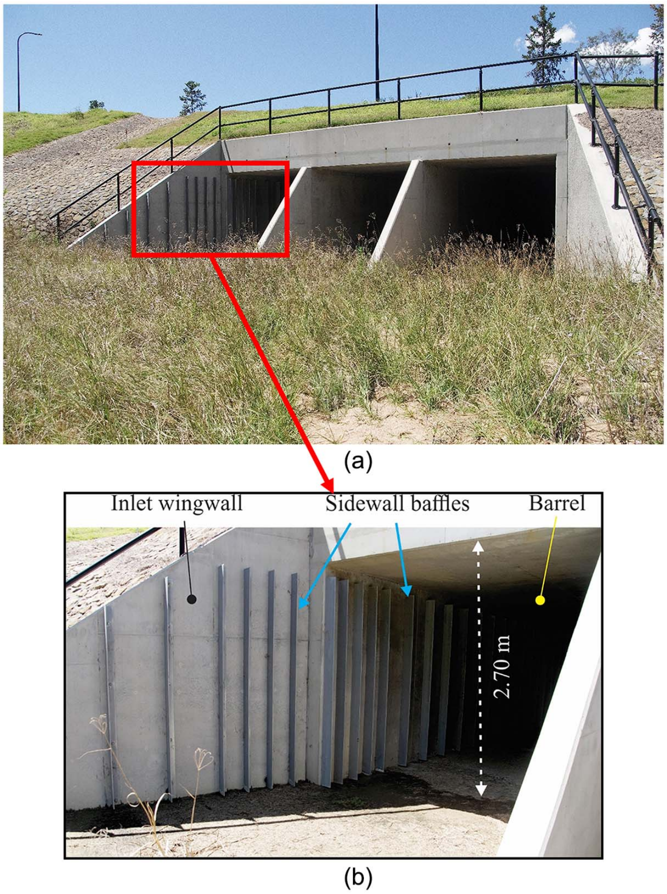

Fig. 1. (a) Inlet of multicell box culvert equipped with full-height sidewall baffles in eastern Australia (Flagstone QLD, Australia) on October 2, 2021; and (b) details of culvert inlet and barrel start with sidewall baffles (baffle width $h_b = 0.150$ m, and cavity length $L_b = 0.60$ m) installed to assist with upstream fish passage.

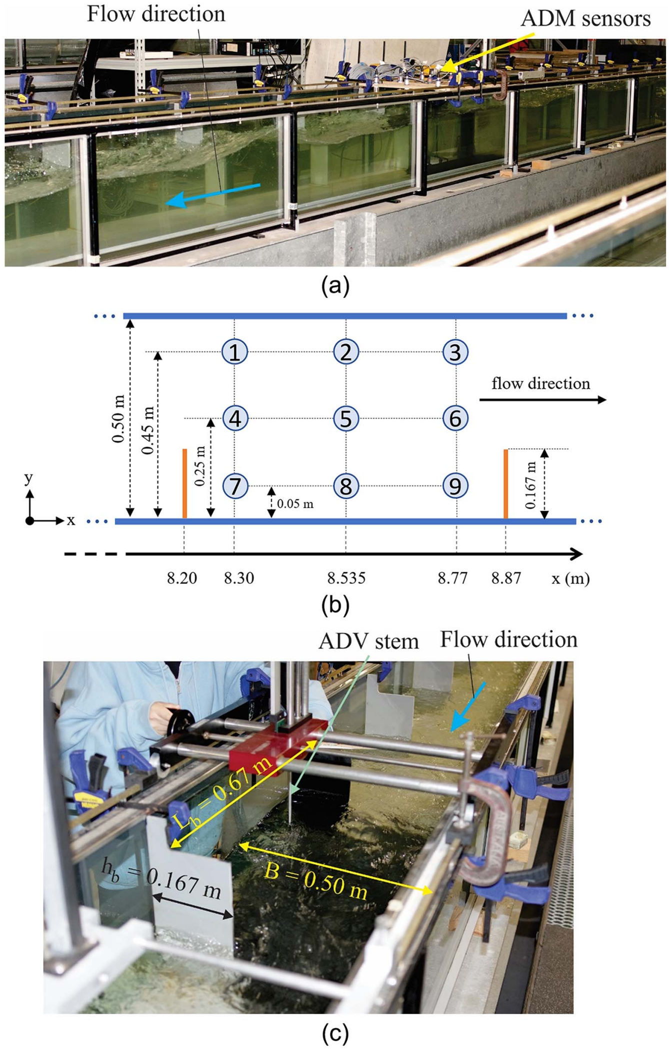

Fig. 2. Physical modeling of box-culvert barrel equipped with full-height sidewall baffles: (a) free-surface measurements for $Q = 0.092$ m^3/s, showing the ADM sensors and large wave motion; (b) horizontal locations of ADM sensors 1–9 (not to scale); and (c) velocity measurements for $Q = 0.056$ m^3/s, showing the ADV. Flume geometry: $B = 0.5$ m, $L_b = 0.67$ m, and $h_b = 0.167$ m.

optimal fishway design, considering the recirculation zones and hydrodynamic instabilities introduced by sidewall baffles.

Experimental Facility, Instrumentation, and Methodology

Experimental Facility

The physical experiments were conducted in a relatively large facility, previously used by Leng and Chanson (2020a). This facility is a near-full scale individual culvert barrel within a common multicell box culvert. The extrapolation of the data to large culvert structures was based upon a combined Froude and Morton similitude (Chanson and Gualtieri 2008; Pfister and Hager 2014), with a geometric scale ratio $L_r = 1$–4 for typical precast concrete units with internal widths between 0.5 and 2 m used for culvert construction, where L_r is the ratio of prototype to model dimensions.

The laboratory experiments were conducted in a 15-m-long × 0.5-m-wide horizontal channel (Fig. 2). The invert was made of smooth PVC, and the sidewalls were transparent tempered glass. The water discharge was supplied to the flume through a 2.0-m-long × 1.25-m-wide intake structure equipped with a succession of baffles, flow straighteners, and a three-dimensional convergent section leading to the 0.5-m-wide channel. The flow rate was provided by a water reticulation system equipped with a constant-head reservoir. The channel ended with a free overfall at its downstream end.

Relatively large full-height sidewall baffles ($h_b = 0.167$ m) were placed in the rectangular channel along the right sidewall, where h_b is the baffle size in the direction normal to the sidewall (Fig. 2). The baffles were plain and rectangular, and fixed to the false floor and held at the top; clay was used to seal the gaps between the baffles and sidewall. The relatively large baffle width was chosen to highlight their protrusion effects in the main channel. Two configurations of baffle spacing were tested: the longitudinal interval between adjacent baffles was set at $L_b = 0.67$ m in the first configuration, and $L_b = 0.33$ m in the second configuration.

Instrumentation

The discharge was measured with a Venturi meter installed in the pipe of the reticulation system. The Venturi was built based upon British Standards Institution (1943), and the error of the flow rate was less than 2%. The water elevation on the channel centerline was measured with a pointer gauge, with an accuracy of ±0.5 mm. The time series of the water surface elevation were recorded using two independent methods: video recordings with backlighting through the sidewalls, and acoustic displacement meter (ADM) sensors installed above the channel [Figs. 2(a and b)]. Two video cameras were used: a Casio (Shibuya, Tokyo) EX-10 operating at 120 frames/s, and a Sony (Minato City, Tokyo) RX100V at 100 frames/s. A set of Microsonic (Dortmund, Germany) Mic + 25 ADMs was sampled simultaneously and synchronously at 200 Hz.

The water velocities were recorded with a Nortek (Rud, Norway) Vectrino + acoustic Doppler velocimeter (ADV) and a three-dimensional (3D) side-looking head. The ADV signal was sampled at 200 Hz for 180 s at each measurement point. The vertical translation of the ADV unit was controlled by a fine-adjustment screwdriver mechanism connected to a Mitutoyo (Kawasaki, Kanagawa, Japan) digital scale unit, with an accuracy of ±0.1 mm. The accuracy of the longitudinal and transverse positions was less than 2 mm. The ADV time-series data were postprocessed to remove erroneous data and spikes, which mainly were introduced by low concentration of suspended sediment particles. Data points with an average correlation of less than 60% and/or average signal-to-noise ratio (SNR) less than 5 dB were removed. The signal was despiked further using a phase-space thresholding technique (Goring and Nikora 2002; Wahl 2003; Mori et al. 2007).

Triple Decomposition of Free-Surface and Velocity Data

The instantaneous water depth (d) and velocity (V) signals indicated the presence of seiching in the form of low-frequency oscillations. The characteristic periods were about 1–3 s, depending upon the flow and boundary conditions. A typical frequency analysis of the signal is presented in Fig. 3. A triple decomposition of the instantaneous signal data was implemented based upon previous studies in riverine systems (Hussain and Reynolds 1972; Fox et al. 2005; Brown and Chanson 2013). For completeness, the triple decomposition also was applied to estuarine flows (Suara et al. 2019), following previous applications (Trevethan et al. 2008), as well as to two-phase gas–liquid flows (Felder and Chanson 2014; Wang et al. 2014).

The instantaneous time series, e.g., of the velocity signal, may be represented as a superposition of three components

$$V = \langle V \rangle + [V] + \{V\} \tag{1}$$

where V = instantaneous velocity measurement; $< V >$ = low-pass filtered contribution; $[V]$ = band-pass-filtered or slow-fluctuation component; and $\{V\}$ = high-pass-filtered component corresponding to true turbulence. The triple decomposition application requires the selection of physically meaningful cut-off frequencies, f_1 and f_2, where f_1 is the upper cut-off frequency of the low-pass filtered component and f_2 is the lower cut-off frequency of the high-pass filtered signal. A detailed sensitivity analysis was performed (Hu et al. 2022), and the results indicated that the mean contribution $< V >$ was little affected by a cut-off frequency $f_1 < 1/3 \times f_d$, where f_d is the dominant frequency (Fig. 3), whereas the high-frequency turbulent component $\{V\}$ was almost independent of an upper cut-off frequency $f_2 > 3 \times f_d$. Herein, the same triple decomposition technique was applied to both instantaneous free-surface elevation and velocity components using $f_1 = 1/3 \times f_d$ and $f_2 = 3 \times f_d$.

Experimental Flow Conditions

The physical experiments were conducted in the horizontal channel, acting as a large box culvert barrel model for two longitudinal baffle spacings across a relatively wide range of flow conditions (Table 1). Basic observations and centerline free-surface measurements were

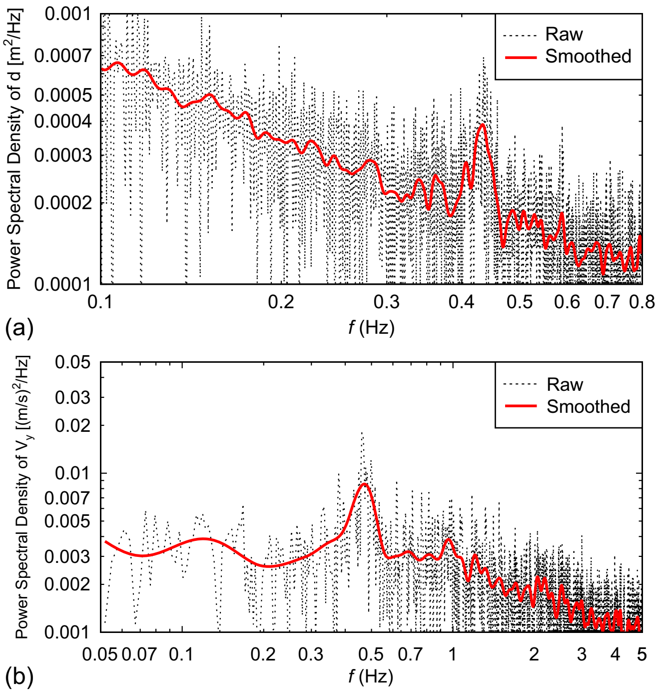

Fig. 3. Frequency analyses of instantaneous free-surface elevation and velocity data in a culvert barrel channel equipped with full-height sidewall baffles: (a) free-surface elevation, for flow conditions $Q = 0.0556\ \mathrm{m^3/s}$, $x_b = 8.2$ m, $L_b = 0.667$ m, and $h_b = 0.167$ m at location $(x - x_b)/L_b = 0.5$, $y/B = 0.5$; and (b) transverse velocity component for flow conditions $Q = 0.0556\ \mathrm{m^3/s}$, $x_b = 8.2$ m, $L_b = 0.667$ m, and $h_b = 0.167$ m at location $(x - x_b)/L_b = 0.5$, $y/B = 0.06$, $z/d_o = 0.04$ (x = longitudinal coordinate starting from the upstream end of the flume; y = transverse coordinate starting from the right sidewall; z = vertical coordinate starting from the PVC false floor; and $x_b = 8.20$ m indicates the longitudinal location of the upstream baffle of the test cavity).

undertaken along the whole channel length for unit discharges $0.057\ \mathrm{m^2/s} < q < 0.19\ \mathrm{m^2/s}$, with various characteristic water depths $0.125\ \mathrm{m} < d_o < 0.286$ m. Instantaneous measurements of water depth d and velocity V were obtained in three cavities, located at $6.19\ \mathrm{m} < x < 6.86$ m, $8.20\ \mathrm{m} < x < 8.87$ m, and $8.20\ \mathrm{m} < x < 8.53$ m, where x is the longitudinal location measured from the upstream end of the channel. Table 1 summarises the experimental flow conditions and corresponding measurements.

Flow Patterns

Presentation

For all water discharges (Table 1), the open-channel flow in the baffled channel was very turbulent (Reynolds number $\mathrm{R} = 1.51 \times 10^5$–$3.45 \times 10^5$). The water free-surface had a tumbling appearance, typical of natural stream torrents, although the laboratory conditions were subcritical, with Froude number $\mathrm{Fr} < 0.4$ (Fig. 2). Large-scale coherent structures were generated by the baffles, and dye injection highlighted some complicated recirculation motion in the baffle cavities. Large water surface elevation fluctuations were observed in both main stream and cavity regions. The main flow propagated downstream at relatively high velocities, past the cavity regions between adjacent sidewall baffles. Some stagnation regions were observed on the upstream side of the baffles, locally

Table 1. Detailed investigations of box culvert barrel model equipped with full-height sidewall baffles

θ (degrees)	B (m)	h_b (m)	Measurements	x_b (m)	L_b (m)	L_b/h_b	q (m^2/s)	d_o (m)	R
0	0.5	0.167	Free-surface measurements (ADM)	8.20	0.67	4	0.0578–0.184	0.135–0.286	1.5×10^5–3.4×10^5
			Free-surface measurements	8.20	0.67	4	0.0578–0.184	0.135–0.286	1.5×10^5–3.4×10^5
			(Side view)	6.19	0.67	4	0.0578	0.158	1.4×10^5
			ADV velocity measurements	8.20	0.67	4	0.0578–0.111	0.135–0.202	1.5×10^5–2.4×10^5
				8.20	0.33	2	0.0578–0.111	0.125–0.192	1.5×10^5–2.5×10^5

Note: θ = channel slope angle; d_o = characteristic water depth in main flow; B = internal channel width; and R = Reynolds number defined in terms of hydraulic diameter.

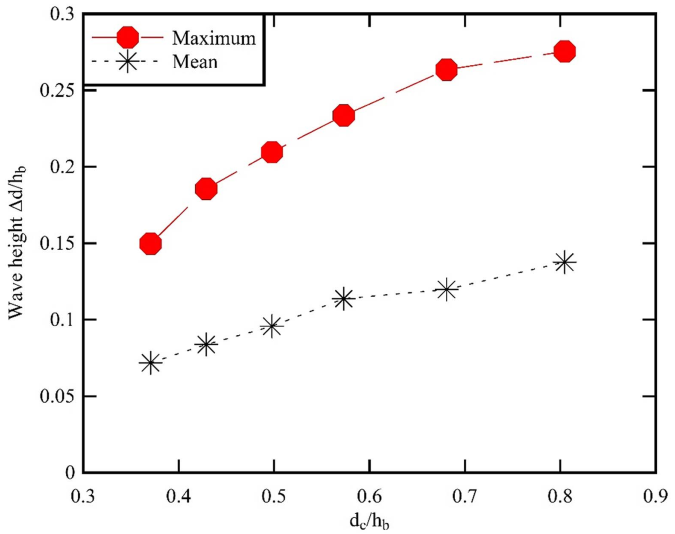

Fig. 4. Dimensionless mean and maximum wave height derived from surface elevation measurements (ADM 5) as a function of the dimensionless flow rate. Flow conditions: $0.029\ \mathrm{m^3/s} < Q < 0.0925\ \mathrm{m^3/s}$, $L_b = 0.67$ m, and $L_b/h_b = 4$.

creating an increased free-surface elevation at the upstream corner. Separation took place at the outer edge of each baffle, inducing cross-waves propagating downstream.

Altogether, the water surface was unstable, very rough, and constantly fluctuating [Figs. 2(a) and 4]. Fig. 4 presents some typical results from the measurements of ADM 5, demonstrating the dimensionless mean and maximum wave heights as a function of the dimensionless discharge d_c/h_b, where d_c is the critical flow depth. For comparison, experiments in the smooth channel flow without baffles yielded much smaller free-surface roughness of about ±0.5 mm (i.e., $\pm 0.003 \times h_b$). Herein, the maximum wave height was about twice the value of the mean wave height, and the maximum wave heights were approximately 20% of the mean water depths in the presence of full-height sidewall baffles. Large-scale turbulent structures and surface scars were seen at the free surface throughout the whole channel. Some complicated recirculation motion behind the baffles was seen for the full cavity length. These were investigated specifically using neutrally-buoyant particles (Li and Chanson 2020).

Free-surface instabilities were observed for the full length of the channel [Fig. 2(a)]. The water depth constantly oscillated with time in the mainstream as well as in the baffle cavities. The surface instabilities created some considerable amount of wave breaking and local air bubble entrainment, especially at larger discharges. Based upon the nonintrusive instantaneous water elevation signals, the dominant frequency f_d of water surface oscillations was found to

Table 2. Characteristic frequency f_d of instantaneous water surface and velocity oscillations derived from fast Fourier transfer analyses for $x_b = 8.20$ m

L_b (m)	L_b/h_b	q (m^2/s)	d_o (m)	f_d (Hz)	R	$f_d \times L_b/V_o$[a]
0.67	4	0.0578	0.132	0.36	1.51×10^5	0.55
		0.072	0.156	0.38	1.77×10^5	0.55
		0.090	0.180	0.42	2.09×10^5	0.56
		0.111	0.204	0.44	2.44×10^5	0.54
		0.144	0.245	0.47	2.90×10^5	0.53
		0.185	0.286	0.50	3.45×10^5	0.52
0.33	2	0.0578	0.125	0.83	1.54×10^5	0.59
		0.111	0.192	0.47	2.51×10^5	0.27

Note: d_o = characteristic water depth in main flow; R = Reynolds number defined in terms of hydraulic diameter; and V_o = cross-sectional-averaged bulk velocity.
[a]Dominant frequencies for instantaneous free-surface and/or velocity oscillations.

be identical in the main stream and the lateral cavity. The characteristic frequency of water surface fluctuations was identical to the characteristic oscillation frequency of the velocities for the same flow conditions with both instantaneous measurements of free-surface elevation and velocity. Typical results are reported in Table 2.

Wall Roughening and Flow Resistance

The culvert barrel roughening with full-height sidewall baffles generated some low-velocity areas to assist with upstream fish migrations. Such a design has not been popular among local governments and road departments because of its negative effects on the hydraulic conveyance (Leng and Chanson 2020b; Dutton et al. 2021). Herein, the longitudinal free-surface profile was measured along the channel centerline, and the data were compared with the theoretical profile based on backwater equation. The Darcy–Weisbach friction factor f was derived from the backwater calculation profile that best-fit the measured free-surface profile (Li and Chanson 2020).

In this study, the best-fit backwater profile was achieved with $f \sim 0.3$, compared with a smooth unbaffled channel flow resistance of about $f \sim 0.015$–0.02 (Fig. 5). Simply, the full-height sidewall baffles increased the Darcy–Weisbach friction factor by more than 1 order of magnitude. The baffled channel data further showed an increased flow resistance with increasing Reynolds number (Fig. 5). That is, the data set indicated an increasing friction factor with increasing discharge. Physically, the influence and impact of the full-height lateral baffles on the flow increased with increasing water depth, and hence discharge, as the volume of recirculating cavity fluid became comparatively larger with higher water depth in a comparatively narrower channel.

J. Hydraul. Eng., 2024, 150(4): 04024010

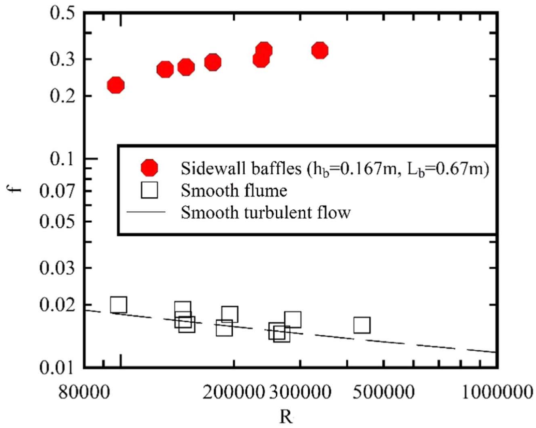

Fig. 5. Flow resistance between smooth channel and channel equipped with full-height sidewall baffles ($L_b = 0.67$ m, $h_b = 0.167$ m). Smooth channel data sets: Cabonce et al. (2019) and present study; sidewall baffled channel data sets: Leng and Chanson (2020a) and present study.

In terms of the Gauckler–Manning coefficient, this would represent an increase by a factor of 5. However, the use of the empirical Gauckler–Manning coefficient in artificial channels may be incorrect: "The (Gauckler–Manning) equations express our continuing ignorance of turbulent processes" (Liggett 1975, p. 45); "Although these several [Bazin and Manning] expressions are in general use in many countries, ... they are at best empirical relationships with scarcely a trace of analytical foundation. The danger in such methods is self-evident" (Rouse 1938, pp. 280–281); and "Flow resistance calculations in open channels must be performed in term of the Darcy friction factor" (Chanson 2004, pp. 81–82).

Velocity Distributions

Presentation

Detailed velocity data were collected at three longitudinal locations, with over 200 sampling points per cross section at a specific longitudinal location, for a given flow condition. Typical data are shown in Fig. 6. In this study, x is the longitudinal coordinate positive downstream, with $x = 0$ at the upstream end of the channel; y is the transverse coordinate, with $y = 0$ at the right sidewall; z is the vertical coordinate, with $z = 0$ at the invert; V_x is the longitudinal velocity component, which is positive downstream; V_y is the transverse velocity component, which is positive toward the left sidewall; and V_z is the vertical velocity component, which is positive upward. The longitudinal location of the upstream baffle of the test cavity is denoted x_b.

All the longitudinal velocity measurements presented a mean trend which was consistent with previous Prandtl–Pitot tube data obtained with a slightly different baffle configuration ($h_b = 0.083$ m, $L_b = 0.333$ m, and $Q = 0.054$ m^3/s) (Leng and Chanson 2020a). However, the current data set provided a finer level of detail owing to the high temporal resolution of the ADV system and ability to record instantaneous negative velocities. The velocity measurements showed a drastic impact of lateral baffles on the entire velocity field. Compared with a smooth channel flow without baffles, slower velocities and higher water depths were observed. The sidewall baffles modified the vertical profiles of streamwise velocity on the channel centerline [Fig. 6(a)]. In a smooth unbaffled channel, a partially developed turbulent boundary layer flow was observed with an ideal fluid flow region above (Leng and Chanson 2020a). The present centerline data highlighted a velocity maximum at about $z/d_o \sim 0.45$–0.5, with a marked velocity dip next to the water surface. Moreover, in the wake of the full-height sidewall baffles, i.e., $0 < y \ll h_b$, a recirculation region with negative velocities was recorded.

Typical contour maps of time-averaged velocities are shown in Figs. 6(b and c), which show the detailed velocity field in the cavity and shear regions. The longitudinal velocity component data indicated three distinctive regions: (1) a well-marked high-velocity region for $h_b \ll y < B$; (2) a shear region with large transverse velocity gradient $\partial V_x/\partial y$ downstream of the outer edge of the baffle ($y \sim h_b$); and (3) a recirculation region with negative velocities for $0 < y \ll h_b$ [Fig. 6(b)]. The time-averaged negative velocities reached values as low as -0.15 m/s. Although the transverse velocities had magnitudes smaller than the streamwise velocity components, the transverse velocity data implied some strong secondary current pattern, especially in the shear region [Fig. 6(b)].

The longitudinal velocity measurements were checked for the conservation of mass by comparing the measured water discharge Q to the integration of time-averaged longitudinal velocities assuming a no-slip condition at the invert and on both sidewalls

$$Q = \iint_A V_x \times dz \times dy \tag{2}$$

where A = flow cross-section area. The results indicated that the equation of conservation of mass Eq. (2) was fulfilled within less than 7% deviation. Moreover, the time-averaged transverse velocity data were integrated over the flow cross section to check the no-flow-through condition

$$\iint_A V_y \times dz \times dy = 0 \tag{3}$$

The data showed a reasonable agreement in terms of Eq. (3), with a maximum deviation of 5% of the discharge. A continuity check was not meaningful in terms of the vertical velocity data, owing to the highly unsteady free-surface with large-amplitude oscillations.

Shear Region

The flow past a sidewall baffle may be idealized by a two-dimensional supported jet, discharging through a nozzle of breadth $B - h_b$ and expanding into a confined space of total width B. The equations of conservation of mass and momentum may be developed neglecting energy and momentum loss in first instance. Although several theoretical models of flow in recirculation cavities have been developed (Kimura and Hosoda 1997; Mizumura and Yamasaka 2002), a simpler theoretical model of the recirculation velocity profile was proposed, associated with gyres and dead zones in river channels with lateral cavity (Hill 2014). Applying the model of Hill (2014) based on the assumptions that (1) the gyre diameter is equal to the baffle size h_b; and (2) the dimensionless interfacial shear along the cavity is about equal to the dimensionless total drag, the predicted velocity distributions in the lateral cavity were calculated (Fig. 7). Fig. 7 shows the theoretical and the measured depth-averaged velocities. Although Hill's (2014) model was not developed for long lateral cavities, the results had relatively close agreement with the present data (Fig. 7).

Velocity Fluctuations

The velocity fluctuations were represented by the standard deviations of velocity components in three directions. The flow was very

J. Hydraul. Eng., 2024, 150(4): 04024010

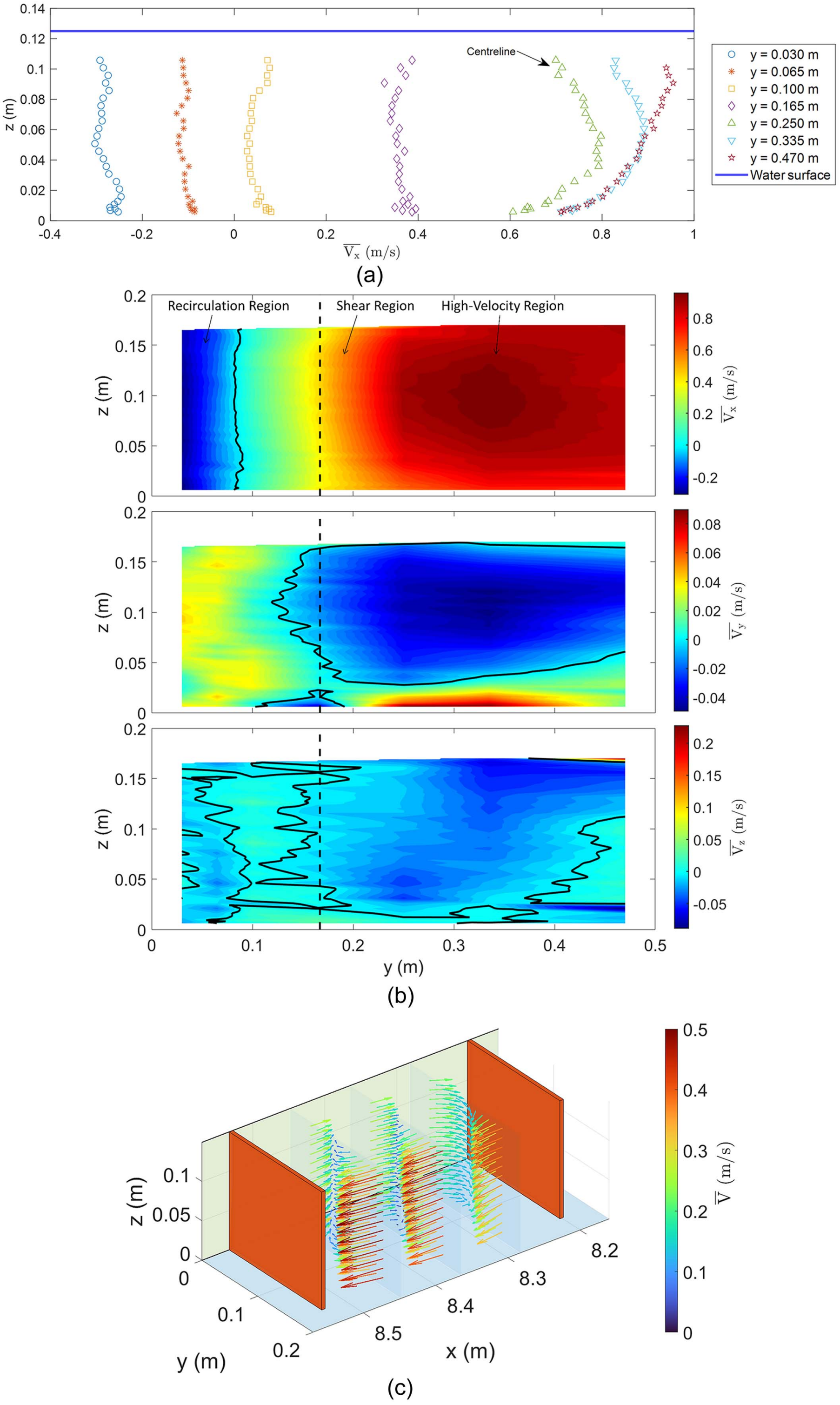

Fig. 6. Time-averaged velocity field: (a) vertical profiles of time-averaged longitudinal velocity for flow conditions $Q = 0.0289$ m^3/s, $L_b = 0.33$ m, $h_b = 0.167$ m, $L_b/h_b = 2$, and $(x - x_b)/L_b = 0.5$; (b) contour maps of time-averaged longitudinal, transverse, and vertical velocity components for $Q = 0.0556$ m^3/s, $x_b = 8.20$ m, $L_b = 0.33$ m, $h_b = 0.167$ m, $(x - x_b)/L_b = 0.5$ (dashed black vertical line indicates outer edge of sidewall baffle; solid black line indicates $\bar{V} = 0$); and (c) time-averaged velocity field in the cavity area for $Q = 0.0556$ m^3/s, $x_b = 8.2$ m, $L_b = 0.33$ m, and $h_b = 0.167$ m (velocity magnitude indicated by shading and length of vector arrow).

turbulent in the sidewall-baffled channel. Large velocity fluctuations were observed in all three directions, and the largest fluctuations typically were in the shear zone located in the wake of the outer edge of the baffle. Large turbulent intensities were recorded, with values of v_x'/V as high as 70%, v_y'/V as high as 30%, and v_z'/V as high as 100%, where V is the cross-sectional-averaged bulk velocity. Typical contour maps of velocity standard deviations are presented in Fig. 8. Two key features were that (1) the maximum transverse velocity fluctuations v_y' in the wake of the outer edge of the baffle ($y \approx h_b$) [Fig. 8(b), arrow]; and (2) the large vertical

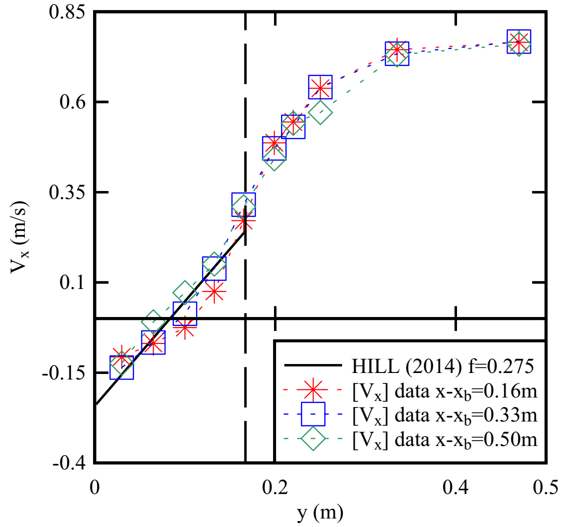

Fig. 7. Transverse distribution of depth-averaged longitudinal velocity in the culvert barrel channel equipped with full-height sidewall baffles, from present experiment data and theoretical model of cavity recirculation of Hill (2014) assuming $f = 0.275$. Dashed black vertical line indicates outer edge of the sidewall baffle. Flow conditions: $Q = 0.029\ \mathrm{m^3/s}$, $x_b = 8.2$ m, $L_b = 0.667$ m, $h_b = 0.167$ m, and $L_b/h_b = 4$.

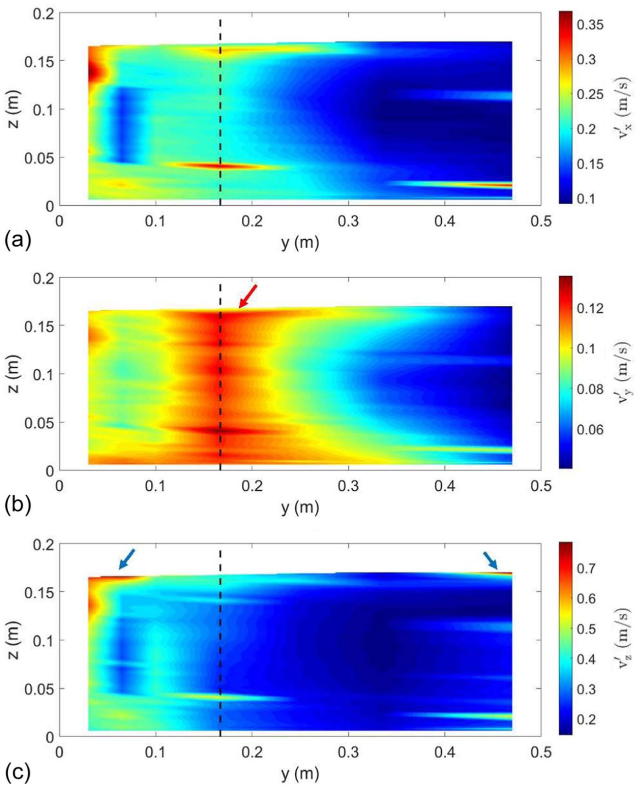

Fig. 8. Contour maps of standard deviations of longitudinal, transverse and vertical velocity components for $Q = 0.0556\ \mathrm{m^3/s}$, $x_b = 8.2$ m, $L_b = 0.33$ m, $h_b = 0.167$ m, $(x - x_b)/L_b = 0.5$: (a) horizontal velocity fluctuations v_x'; (b) transverse velocity fluctuations v_y', maximum in the wake of the outer edge of the baffle ($y \approx h_b$, arrow); and (c) vertical velocity fluctuations v_z', maximum next to the free-surface (arrows). Dashed black vertical lines indicate outer edge of sidewall baffles.

velocity fluctuations v_z' next to the free surface [Fig. 8(c), arrows]. The former was consistent with the large transverse secondary currents in the shear zone and was associated with some momentum transfer from the mainstream to the recirculation region, across the mixing layer, to maintain the recirculation motion. The latter was linked to the large free-surface fluctuations and was associated with large vertical velocity fluctuations next to the free surface, because $V_z = \partial d/\partial t$ at the free surface (i.e., $z = d$).

Although Fig. 8 presents the standard deviations of the complete signal, the triple-decomposed components were calculated for each time series collected at all sampling locations. The outcomes provided a statistical measure of the relative turbulence strength. The standard deviations of the filtered components then were compared with those of the corresponding complete data signals (Fig. 9). In Fig. 9, the horizontal coordinates refer to the standard deviations of the complete signal, and the vertical coordinates represent the standard deviations of the filtered components. The 1:1 line is included in each plot to assist the comparison. In Fig. 9, each dot corresponds to the data collected at a specific sampling location. For each group of filtered data points (e.g., $<d>'$, $[d]'$, and $\{d\}'$), the best fit against the raw data (e.g., d') is shown by the solid lines in Fig. 9.

In terms of free-surface elevation, the band-pass filtered component $[d]$ was the main contributor to the free-surface turbulence induced by the water elevation oscillations. For example, in the data in Fig. 9(a), $<d>' \approx d' \approx 0.28$, $[d]'/d' \approx 0.85$, and $\{d\}'/d' \approx 0.14$. For the velocity data, the low-pass components had the smallest standard deviations in all three components. For the longitudinal and vertical directions, the standard deviations of the high-pass components were the largest with $\{V_x\}'/V_x' \approx 0.62$–$0.77$ and $\{V_z\}'/V_z' \approx 0.83$–$0.90$ on average. The band-pass-filtered turbulent component was lower than the contribution of turbulence from the high-pass components, with $[V_x]'/V_x' \approx 0.36$–0.50 and $[V_z]'/V_z' \approx 0.20$–0.29 on average. However, in the transverse direction, the contributions of the band-pass and high-pass components were almost comparable. That is, $[V_y]'/V_y'$ was nearly equal to $\{V_y\}'/V_y'$ on average.

Overall, the slow oscillations were a major source of free-surface turbulence and a significant contribution to the flow turbulence in the transverse direction. In the longitudinal and vertical directions, the high-frequency fluctuations were the leading sources of turbulent motion.

Discussion: Coupling between Free-Surface and Velocity Motion

The coupling between free-surface and velocity fluctuations was investigated in the wake of the baffle's outer edge ($y = h_b$) by sampling synchronously the ADM and ADV for 5 min at 200 Hz [Fig. 10(a)]. Based upon the instantaneous free-surface elevation data, the free-surface's vertical velocity was derived as $V_s = \partial d/\partial t$. From the cross-correlation R_{si} between the free-surface velocity V_s and the ADV velocity data V_i (where $i = x, y$, or z), the integral cross-correlation time scale was calculated as

$$T_{si} = \int_{\tau=\tau(R_{si}=(R_{si})_{\max})}^{\tau=\tau(R_{si}=0)} R_{si} \times d\tau \qquad (4)$$

with the integration between the time lag for maximum cross-correlation $(R_{si})_{\max}$ and to the first crossing $R_{si} = 0$. A typical example is presented in Fig. 10(b), with the transverse fluid velocity data V_y collected at the middle of the water column ($z/d_o = 0.56$). In Fig. 10(b), the area of the shaded region represents the integral

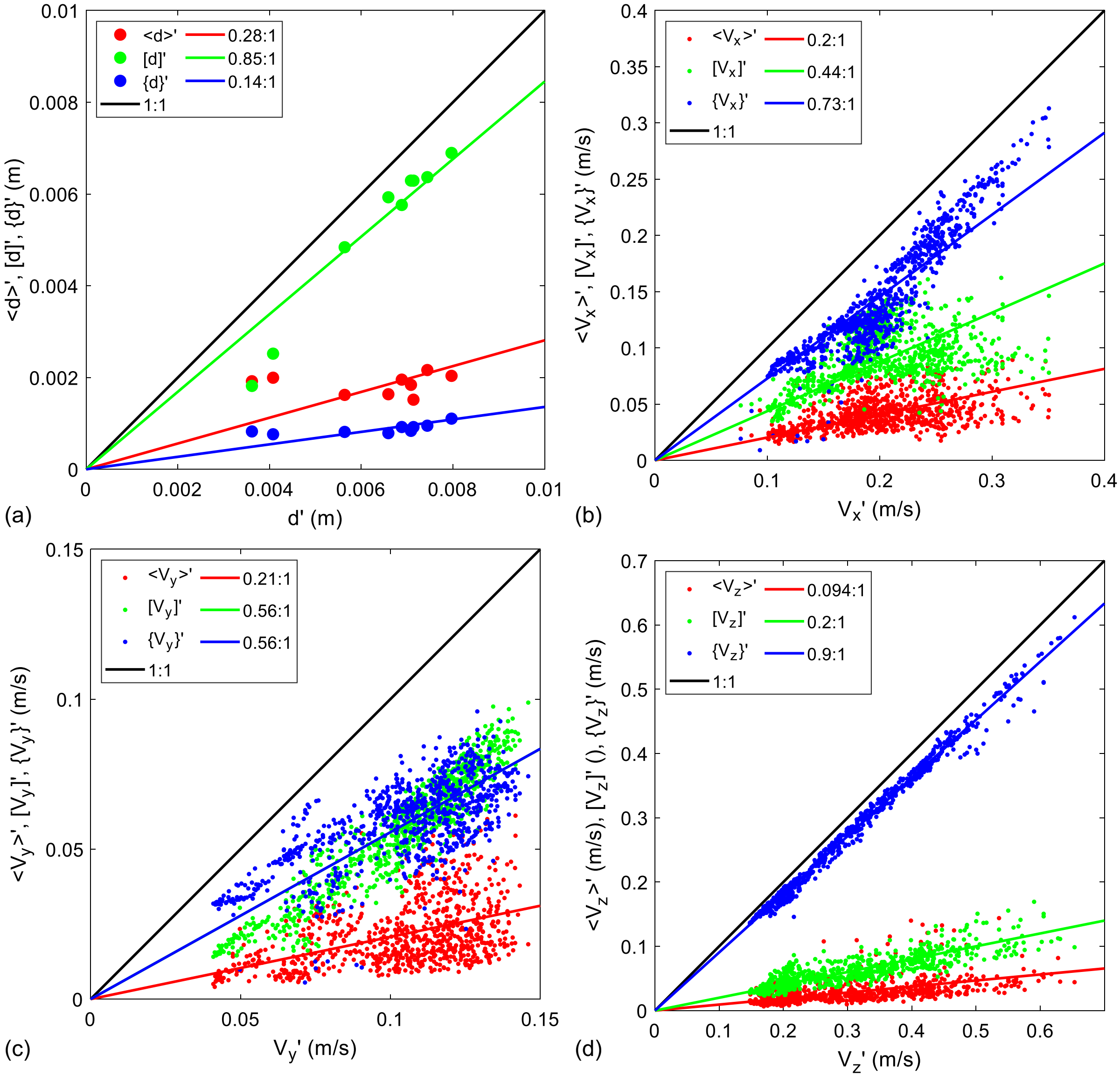

Fig. 9. Standard deviation of filtered data and standard deviation of raw data: (a) free-surface elevation; (b) longitudinal velocity component V_x; (c) transverse velocity component V_y; and (d) vertical velocity component V_z. Black line indicates 1:1 ratio; circles indicate standard deviation for time series from measurements at a physical ADM or ADV sampling location; solid lines indicate best fit for the corresponding categories. Flow conditions: $Q = 0.029$ m^3/s, $L_b = 0.67$ m, and $L_b/h_b = 4$.

time scale T_{sy}. Fig. 10(c) presents typical vertical distributions of the maximum cross-correlation coefficient and integral time scale.

A dominant pattern in terms of maximum cross-correlation was the strong cross-correlation between free-surface fluctuation and the transverse velocity component for the vertical elevations $z/d_o > 0.25$ [Fig. 10(c)]. In terms of integral cross-correlation time scale T_{si}, the transverse fluid component also presented large cross-correlation time scales in response to the free-surface fluctuations in the middle to upper flow region. Such large integral time scales implied some strong coupling and the existence of large coherent structures with vertical axis in the upper part of the flow ($z/d_o > 0.5$).

Conclusion

Detailed measurements of free-surface elevation and turbulent velocity were obtained in a near-full-scale box culvert barrel channel equipped with full-height sidewall baffles on one side. Although the concept originally was proposed to assist the upstream fish passage at small discharges, the asymmetrical baffle arrangement created strong and adverse free-surface and hydrodynamic instabilities at medium to large discharges. The physical observations encompassed relatively slow oscillations in water surface depth in the entire channel, together with large fluctuations of all three velocity components.

The time-averaged velocity data indicated a high-velocity zone beside the baffles, a recirculation region with marked negative velocities in the wake of baffles, and a shear zone between, characterized by intense secondary motion and transverse velocity fluctuations. The water surface elevation and turbulent velocity signals were processed using a triple decomposition method to quantify the relative impact of the slow oscillation on the turbulent fluctuations. For the experimental flow conditions, the slow fluctuations were the major source of free-surface turbulence and turbulent velocity fluctuations in the transverse direction. This was associated with

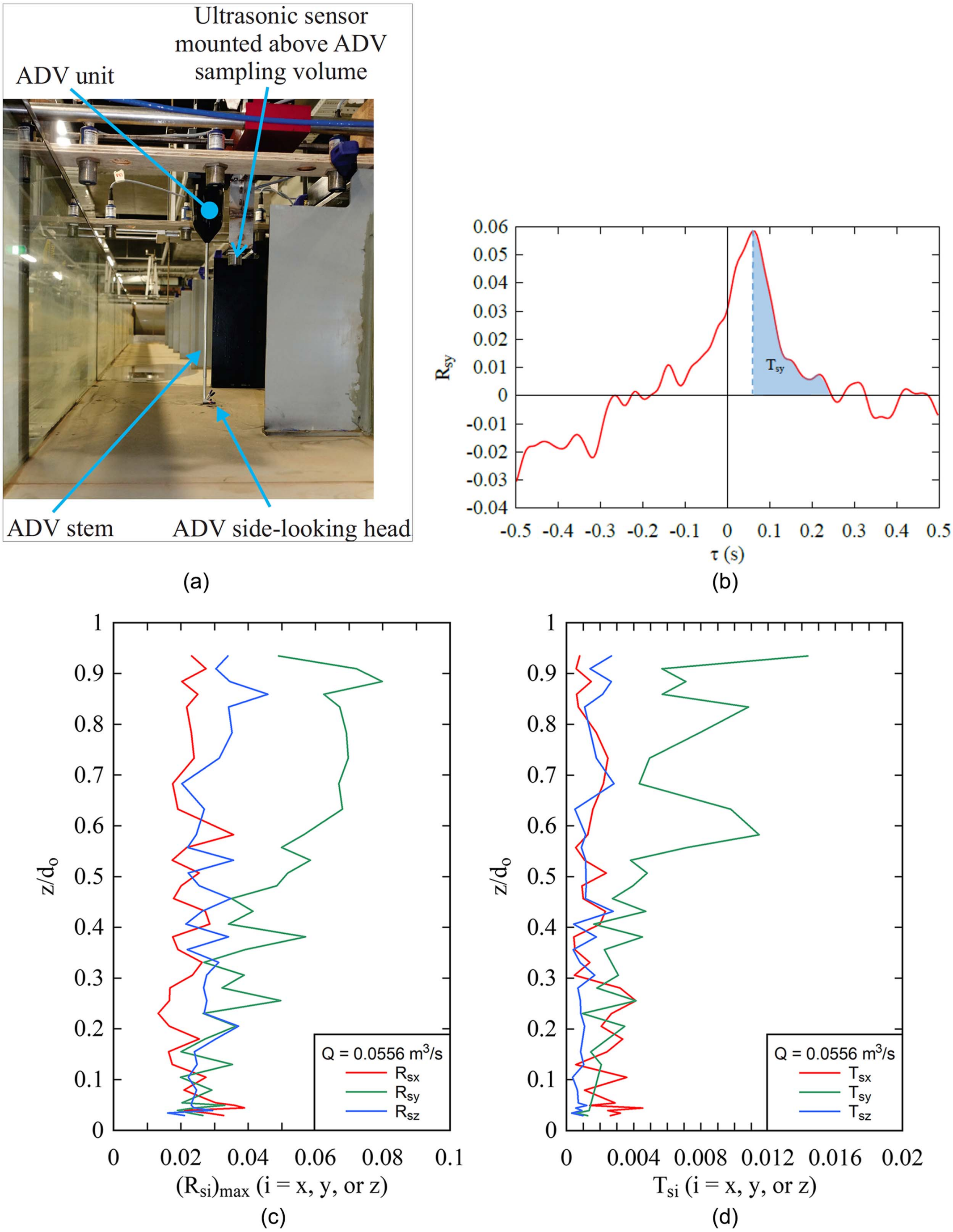

Fig. 10. Coupling between free-surface and velocity fluctuations in the wake of the sidewall baffle's outer edge: (a) ADV unit and ultrasonic acoustic displacement meter setup in the sidewall baffle channel looking downstream; (b) cross-correlation between free-surface velocity V_s and transverse water velocity V_y (area of shadowed region represents cross-correlation time scale T_{sy}); (c) maximum cross-correlation $(R_{si})_{\max}$ at different vertical elevations; and (d) integral time scale T_{si} at different vertical elevations. Flow conditions: $Q = 0.0556\ \mathrm{m}^3/\mathrm{s}$, $L_b = 0.67$ m, $h_b = 0.167$ m, $(x - x_b)/L_b = 0.5$, and $y = h_b$.

a strong coupling in terms of surface and velocity fluctuations, with the largest integral time scales, as well as the maximum cross-correlations, observed between the free-surface's vertical velocity and the transverse velocity component. For the longitudinal and vertical velocity component, the high-frequency fluctuation component was the dominant source of turbulence.

In practical design projects of fish-friendly culverts, the effects of sidewall baffles typically increased the fish traversability at small flow rates. However, the protrusion of sidewall baffles into waterways may significantly change the hydraulic conditions and increase flow instabilities at higher flow rates, which would drastically reduce the conveyance of flow and contrarily impede upstream fish passage. In addition, the installation of baffles and the increase in the number of barrel cells to achieve the same design discharge and afflux normally is linked to greater total construction cost, as well as greater operational maintenance costs of sediment and debris removal. All these problems need to be considered for future studies and prototype designs.

Data Availability Statement

All data, models, or code that support the findings of this study are available from the corresponding author upon reasonable request.

Acknowledgments

The authors thank Dr. Carlos Gonzalez (Queensland Department of Transport and Main Roads), Professor Richard Brown Queensland University of Technology (QUT) and Dr. Hang Wang (Sichuan University) for some helpful comments. The authors acknowledge Jason Van Der Gevel and Stewart Matthews (The University of Queensland) for their technical assistance. The financial support of the Australian Research Council (Grant DP190103379) and Apiary Financial (Grantor RE333704) is greatly acknowledged.

Notation

The following symbols are used in this paper:

A = flow cross-section area (m^2);
B = channel width (m), where $B = 0.5$ m in culvert barrel channel;
d = instantaneous water depth measured normal to invert (m);
d_c = critical flow depth (m);
d_o = characteristic water depth measured normal to invert in main flow (m);
$<d>$ = low-pass-filtered water depth component (m);
$[d]$ = band-pass-filtered water depth component (m);
$\{d\}$ = high-pass-filtered water depth component (m);
Fr = Froude number
f = Darcy–Weisbach friction factor;
f_d = dominant frequency of instantaneous water surface and velocity oscillations (Hz);
f_1 = upper cut-off frequency of low-pass-filtered component (Hz);
f_2 = lower cut-off frequency of high-pass-filtered signal (Hz);
h_b = baffle size in direction normal to sidewall (m);
L_b = longitudinal baffle spacing (m);
L_r = geometric scaling ratio, defined as the ratio of prototype to model dimensions;
Q = water discharge (m^3/s);
q = unit discharge (m^2/s);
R = Reynolds number defined in terms of hydraulic diameter;
R_{si} = cross-correlation coefficient between water and velocity fluctuations;
T_{si} = integral cross-correlation time scale for coupling between water and velocity fluctuations (s);
V = velocity (m/s);
V_s = vertical velocity component (m/s) of free-surface;
V_x = longitudinal velocity component, positive downstream (m/s);
V_y = transverse velocity component, positive toward left sidewall (m/s);
V_z = vertical velocity component, positive upward (m/s);
$<V>$ = low-pass-filtered velocity component (m/s);
$[V]$ = band-pass-filtered velocity component (m/s);
$\{V\}$ = high-pass-filtered velocity component (m/s);
V_o = cross-sectional-averaged bulk velocity (m/s);
v = standard deviation of velocity (m/s);
x = longitudinal coordinate, measured from upstream end of channel (m);
x_b = longitudinal baffle location (m);
y = transverse coordinate, where $y = 0$ at right sidewall (m);
z = vertical coordinate, where $z = 0$ at invert (m);
θ = channel slope angle (degrees); and
τ = time lag (s).

References

British Standards Institution. 1943. *Flow measurement*. BS 1042:1943. London: British Standards Institution.

Brown, R., and H. Chanson. 2013. "Turbulence and suspended sediment measurements in an urban environment during the Brisbane river flood of January 2011." *J. Hydraul. Eng.* 139 (2): 244–253. https://doi.org/10.1061/(ASCE)HY.1943-7900.0000666.

Cabonce, J., R. Fernando, H. Wang, and H. Chanson. 2019. "Using small triangular baffles to facilitate upstream fish passage in standard box culverts." *Environ. Fluid Mech.* 19 (1): 157–179. https://doi.org/10.1007/s10652-018-9604-x.

Cahoon, J. E., T. Mcmahon, A. Solcz, M. Blank, and O. Stein. 2007. *Fish passage in Montana culverts: Phase II—Passage goals*. Rep. No. FHWA/MT-07-010/8181. Washington, DC: Montana DOT.

Chanson, H. 2004. *The hydraulics of open channel flow: An introduction*. 2nd ed. Oxford, UK: Butterworth-Heinemann.

Chanson, H., and C. Gualtieri. 2008. "Similitude and scale effects of air entrainment in hydraulic jumps." *J. Hydraul. Res.* 46 (1): 35–44. https://doi.org/10.1080/00221686.2008.9521841.

Chanson, H., and X. Leng. 2021. "Fish swimming in turbulent waters." In *Hydraulics guidelines to assist upstream fish passage in box culverts*. London: CRC Press.

Cote, A. J., and P. W. Webb. 2015. "Living in a turbulent world—A new conceptual framework for the interactions of fish and eddies." *Integr. Comp. Biol.* 55 (4): 662–672. https://doi.org/10.1093/icb/icv085.

Duguay, J., and R. W. J. Lacey. 2014. "Effect of fish baffles on the hydraulic roughness of slip-lined culverts." *J. Hydraul. Eng.* 141 (1): 04014065. https://doi.org/10.1061/(ASCE)HY.1943-7900.0000942.

Duguay, J. M., R. W. J. Lacey, and T. Castro-Santos. 2019. "Influence of baffles on upstream passage of brook trout and brown trout in an experimental box culvert." *Can. J. Fish. Aquat. Sci.* 76 (Jun): 28–41. https://doi.org/10.1139/cjfas-2017-0453.

Dutton, L., C. Russell, and D. Johannsson. 2021. "Solving a biological problem with a hydraulic solution–Fish passage." In *Proc., Engineering, Innovation, and Technology Forum*, 22. Brisbane, QLD, Australia: QLD Dept. of Transport and Main Roads.

Enders, E. C., T. Castro-Santos, and R. W. J. Lacey. 2017. "The effects of horizontally and vertically oriented baffles on flow structure and ascent performance of upstream-migrating fish." *J. Ecohydraul.* 2 (1): 38–52. https://doi.org/10.1080/24705357.2017.1288555.

Felder, S., and H. Chanson. 2014. "Triple decomposition technique in air–water flows: Application to instationary flows on a stepped spillway." *Int. J. Multiphase Flow* 58 (Jan): 139–153. https://doi.org/10.1016/j.ijmultiphaseflow.2013.09.006.

Fox, J. F., A. N. Papanicolaou, and L. Kjos. 2005. "Eddy taxonomy methodology around submerged barb obstacle within a fixed rough bed." *J. Eng. Mech.* 131 (10): 1082–1101. https://doi.org/10.1061/(ASCE)0733-9399(2005)131:10(1082).

Goring, D. G., and V. I. Nikora. 2002. "Despiking acoustic Doppler velocimeter data." *J. Hydraul. Eng.* 128 (1): 117–126. https://doi.org/10.1061/(ASCE)0733-9429(2002)128:1(117).

Hill, D. F. 2014. "Simple model for the recirculation velocity of open-channel embayments." *J. Hydraul. Eng.* 140 (4): 06014004. https://doi.org/10.1061/(ASCE)HY.1943-7900.0000837.

Hu, J., Y. Li, and H. Chanson. 2022. "Near-full-scale physical modelling and open-channel flow velocity in a fish-friendly culvert with full-height sidewall baffles." In *Proc., 9th IAHR Int. Symp. on Hydraulic Structures ISHS2022*, 411–420. Logan, UT: Utah State Univ.

Hussain, A. K. M. F., and W. C. Reynolds. 1972. "The mechanics of an organized wave in turbulent shear flow. Part 2. Experimental results." *J. Fluid Mech.* 54 (2): 241–261. https://doi.org/10.1017/S0022112072000667.

Jones, P. E., J. C. Svendsen, L. Borger, T. Champneys, S. Consuegra, J. A. H. Jones, and C. Garcia de Leaniz. 2020. "One size does not fit all: Inter- and intraspecific variation in the swimming performance of contrasting freshwater fish." *Conserv. Physiol.* 8 (1): 1–12. https://doi.org/10.1093/conphys/coaa126.

Kimura, I., and T. Hosoda. 1997. "Fundamental properties of flows in open channels with dead zone." *J. Hydraul. Eng.* 123 (2): 98–107. https://doi.org/10.1061/(ASCE)0733-9429(1997)123:2(98).

Leng, X., and H. Chanson. 2020a. "Asymmetrical wall baffles to assist upstream fish passage in box culvert: Physical modeling." *J. Irrig. Drain. Eng.* 146 (12): 04020037. https://doi.org/10.1061/(ASCE)IR.1943-4774.0001514.

Leng, X., and H. Chanson. 2020b. "How full-height sidewall baffles affect box culvert capacity: Balancing fish passage and discharge requirements." *Australas. J. Water Resour.* 24 (2): 248–256. https://doi.org/10.1080/13241583.2020.1824367.

Li, Y., and H. Chanson. 2020. "Hydrodynamic instabilities in open-channel flow past lateral cavities." In *Proc., 22nd Australasian Fluid Mechanics Conf. AFMC2020*. Brisbane, QLD, Australia: Univ. of Queensland.

Liggett, J. A. 1975. "Basic equations of unsteady flow." In *Unsteady flow in open channels*, 29–62. San Francisco: Water Resources Publications.

Marsden, T. 2015. *Common rail proof of concept and baffle field trial assessment report*. Rep. to Ocean Watch Australia. Geneva: Australasian Fish Passage Services.

Mizumura, K., and M. Yamasaka. 2002. "Flow in open-channel embayment." *J. Hydraul. Eng.* 128 (12): 1098–1101.

Mori, N., T. Suzuki, and S. Kakuno. 2007. "Noise of acoustic Doppler velocimeter data in bubbly flows." *J. Eng. Mech.* 133 (1): 1–4. https://doi.org/10.1061/(ASCE)0733-9399(2007)133:1(122).

Nikora, V. I., J. Aberle, B. J. F. Biggs, I. G. Jowett, and J. R. E. Sykes. 2003. "Effects of fish size, time-to-fatigue and turbulence on swimming performance: A case study of *Galaxias maculates*." *J. Fish Biol.* 63 (6): 1365–1382. https://doi.org/10.1111/j.1095-8649.2003.00241.x.

Pavlov, D. S., A. I. Lupandin, and M. A. Skorobogatov. 1994. "Influence of flow turbulence on critical flow velocity for gudgeon (*Gobio gobio*)." *Doklady Biol. Sci.* 336 (1): 215–217.

Pfister, M., and W. H. Hager. 2014. "History and significance of the Morton number in hydraulic engineering." *J. Hydraul. Eng.* 140 (5): 02514001. https://doi.org/10.1061/(ASCE)HY.1943-7900.0000870.

Rajaratnam, N., C. Katopodis, and S. Lodewyk. 1991. "Hydraulics of culvert fishways IV: Spoiler baffle culvert fishways." *Can. J. Civ. Eng.* 18 (1): 76–82. https://doi.org/10.1139/l91-010.

Rouse, H. 1938. *Fluid mechanics for hydraulic engineers*. New York: McGraw-Hill.

Suara, K., R. Brown, and H. Chanson. 2019. "Characteristics of flow fluctuations in a tide-dominated estuary: Application of triple decomposition technique." *Estuarine Coastal Shelf Sci.* 218 (Jun): 119–130. https://doi.org/10.1016/j.ecss.2018.12.006.

Trevethan, M., H. Chanson, and R. Brown. 2008. "Turbulence characteristics of a small subtropical estuary during and after some moderate rainfall." *Estuarine Coastal Shelf Sci.* 79 (4): 661–670. https://doi.org/10.1016/j.ecss.2008.06.006.

Tuna, B. A., E. Tinar, and D. Rockwell. 2013. "Shallow flow past a cavity: Globally coupled oscillations as a function of depth." *Exp. Fluids* 54 (Aug): 1586. https://doi.org/10.1007/s00348-013-1586-3.

Valentine, E. M., and I. R. Wood. 1979. "Experiments in longitudinal dispersion with dead zones." *J. Hydraul. Div.* 105 (8): 999–1016. https://doi.org/10.1061/JYCEAJ.0005265.

Wahl, T. L. 2003. "Discussion of 'Despiking acoustic doppler velocimeter data' by Derek G. Goring and Vladimir I. Nikora." *J. Hydraul. Eng.* 129 (6): 484–487. https://doi.org/10.1061/(ASCE)0733-9429(2003)129:6(484).

Wang, H., S. Felder, and H. Chanson. 2014. "An experimental study of turbulent two-phase flow in hydraulic jumps and application of a triple decomposition technique." *Exp. Fluids* 55 (7): 1775. https://doi.org/10.1007/s00348-014-1775-8.